Inorganic Chemistry
Cite This: *Inorg. Chem.* XXXX, XXX, XXX−XXX
Article
pubs.acs.org/IC

Ligand Isomerism in Coordination Cages

Hareesha Dasary, Rajamony Jagan, and Dillip Kumar Chand*

Department of Chemistry, Indian Institute of Technology Madras, Chennai 600036, India

Supporting Information

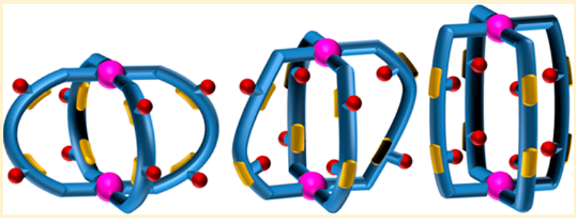

ABSTRACT: Complexation reactions of palladium(II) nitrate with a set of 3-pyridyl appended nonchelating bidentate ligands possessing regioisomeric phenylene-diurea functionalities as spacers were carried out. The ligands utilized in this study are 1,1′-(1,2-phenylene)bis(3-(pyridin-3-yl)urea), **L1**; 1,1′-(1,3-phenylene)bis(3-(pyridin-3-yl)urea), **L2**; and 1,1′-(1,4-phenylene)bis(3-(pyridin-3-yl)urea), **L3**. The complexation reactions of the ligands (**L1**, **L2**, and **L3**) with palladium(II) produced single discrete isomeric cages (**1**, **2**, and **3**) of Pd_2L_4 formulation in each case and thereby illustrated ligand-isomerism in coordination cages. All 16 hydrogen atoms of eight urea moieties present in four ligand strands are delineated completely endohedrally in cage **1** and completely exohedrally in cage **3**, whereas cage **2** exhibited half of the urea hydrogens in exohedral locations and the remaining half in endohedral locations. In addition to the variable number of solvent molecules, the cavities of cages **1** and **2** lodged four and two nitrate ions, respectively, using the endohedral $(H)_{urea}$ atoms (i.e., NH groups) as binding sites, whereas the cavity of **3** remained anion free. The abilities of the complexes **1**−**3** for adsorption of CO_2 gas are demonstrated, and their behaviors are compared.

■ INTRODUCTION

Combination of palladium(II) with selected nonchelating bidentate or polydentate ligands under suitable reaction conditions is a reliable strategy for the preparation of a variety of self-assembled coordination cages of Pd_mL_n formulations.[1−6] However, the general formula of the cages obtained from palladium(II) and a nonchelating bidentate ligand is Pd_mL_{2m} in which the value of "m" is usually dictated by the relative directions of the two coordination vectors of the ligand moiety.[1−33] It can be stated that the more diverged the coordination vectors of the ligand the higher is the nuclearity of the ensuing Pd_mL_{2m} cage. The formula of known Pd_mL_{2m} type cages are as varied as Pd_2L_4,[1,3,4,6−18] Pd_3L_6,[6,19−24] Pd_4L_8,[1,6,19,23,24] Pd_5L_{10},[19] Pd_6L_{12},[5,6,19,25−27] Pd_7L_{14} (optimized),[19] Pd_8L_{16} (not isolated),[28] Pd_9L_{18},[28] $Pd_{12}L_{24}$,[5,6,29−31] $Pd_{24}L_{48}$,[5,6,20,29] $Pd_{30}L_{60}$,[32,33] and $Pd_{48}L_{96}$.[32]

The Pd_2L_4 type cages are simplest among the Pd_mL_{2m} series, yet the most explored. Structural diversity of these binuclear cages is broadly covered under helical or nonhelical architectures. A variety of functional aspects of such binuclear cages are studied by tuning the steric and electronic nature of the exo-/endohedral space of the architectures. The three-dimensional cavity of Pd_2L_4 type cages has been exploited for binding diverse guests such as dye molecules,[7] fullerenes,[14] radical initiators,[12] metal complexes,[13] and anions.[10,17] The formation of isomeric pairs of Pd_2L_4 cages from a pair of isomeric ligands (i.e., ligand isomerism in coordination cages) is a rare phenomenon.[15,16] The backbones of two isomeric ligands could be same, and the variable positions of innocent substituents qualifies them as isomers (say Type-I). Alternatively, the backbones of the two isomeric ligands could be very different (say Type-II). It is more obvious to afford isomeric complexes from the combination of a metal ion with the type-I isomeric ligands[15] than that of the type-II ligands.[16]

Utilization of urea functionalized ligands for the construction of Pd_mL_n type cages is limited to a recent example of the Pd_2L_4 type complex.[9] Complexation of *cis*-protected palladium(II) (i.e., PdL′) with selected urea functionalized ligands are reported to construct certain $Pd_xL'_xL_y$ type complexes; there are only a handful of examples[34−38] and they include $PdL'L_2$,[36] $Pd_2L'_2L_2$,[37,38] $Pd_3L'_3L_2$,[35] and $Pd_3L'_3L_3$[34] type designs. A $Pd_6L^a{}_6L^b{}_6$ type complex is known,[34] where L^a and L^b stand for ligands with and without a urea spacer, respectively.

The endohedral spaces of Pd_2L_4 type complexes are usually conducive to anionic guests due to the cationic nature of the space; hence, counteranions are often lodged in the cavity. We considered crafting regioisomeric phenylene-diurea functionalities at the ligand backbones of 3-pyridyl appended bidentate nonchelating ligands and anticipated constructing Pd_2L_4 type cages (Figure 1). It is safe to predict that endohedral delineation of the urea hydrogen atoms (Figure 1a) in a Pd_2L_4 type cage might strongly facilitate encapsulation and endohedral retention of the counteranions. In the same line, we envisioned that exohedral delineation of the urea hydrogens (Figure 1c) might facilitate exohedral dispositions of the counteranions making the endohedral space of the cavity accessible for other suitable guests.

The present work describes complexation behaviors of palladium(II) separately with three nonchelating bidentate ligands that are regioisomers (Scheme 1). The ligands utilized

Received: July 6, 2018

DOI: 10.1021/acs.inorgchem.8b01884

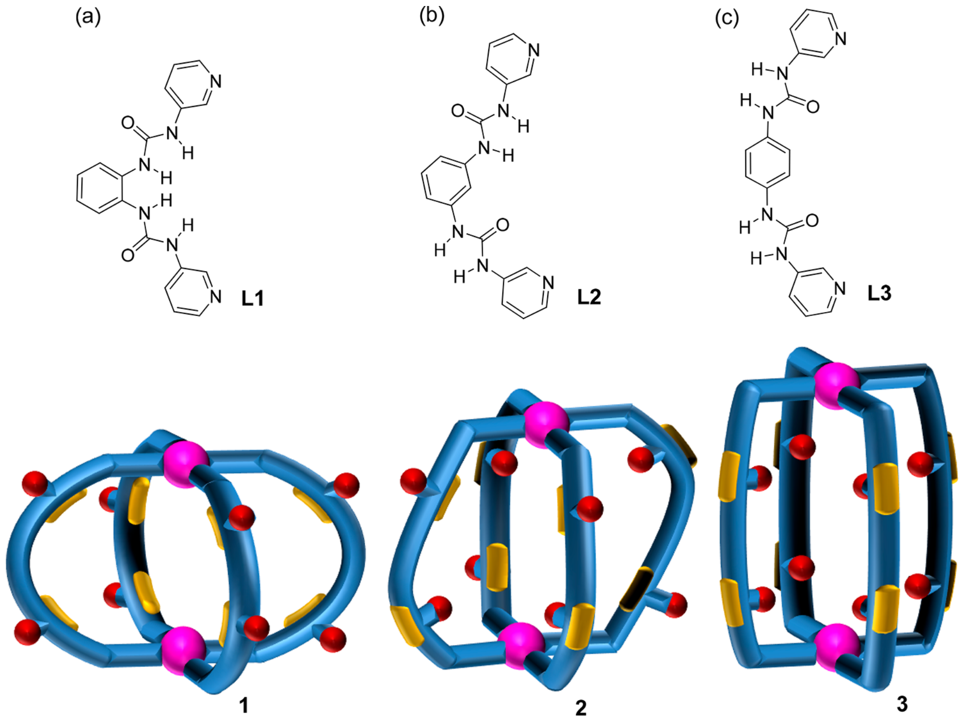

Figure 1. (a−c) Ligand isomerism in Pd_2L_4-type coordination cages (**1**−**3**) perceived from appropriate conformers of regioisomeric ligands (**L1**−**L3**). (Magenta ball: palladium(II); blue rod: nonchelating bidentate ligand; red ball: oxygen of urea; orange strip: anionophilic zone of urea).

are 1,1′-(1,2-phenylene)bis(3-(pyridin-3-yl)urea), **L1**; 1,1′-(1,3-phenylene)bis(3-(pyridin-3-yl)urea), **L2**; and 1,1′-(1,4-phenylene)bis(3-(pyridin-3-yl)urea), **L3**. Crystal structures of the corresponding complexes (**1**, **2**, and **3**) confirmed Pd_2L_4 formulations for each architectures and thereby illustrating ligand-isomerism[39] in the coordination cages using as many as three isomeric ligands. The positions of the urea moieties in the isomeric cages are of particular interest from structural viewpoints. The abilities of the complexes **1**−**3** for adsorption of CO_2 gas are demonstrated and their behaviors are compared.

■ EXPERIMENTAL SECTION

Materials and Methods. $PdCl_2$, nicotinoyl chloride hydrochloride, 1,2-diaminobenzene, 1,3-diaminobenzene, and 1,4-diaminobenzene were acquired from Aldrich; $AgNO_3$, NaN_3, and all common reagents solvents were obtained from Spectrochem, India, and were used as received without further purification. The known ligands **L2**[40] and **L3**[41] were prepared by a slight modification of literature procedures. Nicotinoyl azide required for the synthesis was prepared freshly from nicotinoyl chloride hydrochloride and NaN_3, by following a reported procedure.[38] The deuterated solvents were obtained from Aldrich and Cambridge Isotope Laboratories Inc. ^1H and ^{13}C NMR spectral data were obtained using a Bruker 400 or 500 MHz FT NMR spectrometer in DMSO-d_6 by using TMS in $CDCl_3$ as an external reference. The ESI-MS spectra were obtained from Agilent 6545A Q-TOF and Micromass Q-TOF mass spectrometers. The crystal structures were obtained using a Bruker X8 Kappa X-ray diffraction (XRD) instrument. The powder XRD patterns were obtained using a Bruker D8 Advanced instrument. Thermogravimetric analysis (TGA) data were collected using a Q500 Hi-Res TGA instrument under nitrogen atmosphere, starting from 30 to 910 °C at a heating rate of 20 °C min^{-1}.

Synthesis of the Ligands (L1−**L3).** *General Method.* Nicotinoyl azide (500 mg, 3.37 mmol) and 1,2-diaminobenzene (182 mg, 1.68 mmol) were dissolved in 30 mL of dry CH_3CN under nitrogen atmosphere. The reaction mixture was stirred for 7 h at 70 °C whereupon a white solid was precipitated out. The solid was separated by filtration and washed with CH_3CN and acetone followed by drying under a vacuum to afford the pure ligand **L1**. The ligands **L2** and **L3** were prepared in a similar manner using 1,3-diaminobenzene and 1,4-diaminobenzene, respectively.

1,1′-(1,2-Phenylene)bis(3-(pyridin-3-yl)urea) ***L1***. Yield: (400 mg, 68%). Melting point: 164 °C. ^1H NMR (500 MHz, DMSO-d_6 external TMS/$CDCl_3$): δ = 9.82 (s, 2H, H_e), 9.16 (d, J = 2.3 Hz, 2H, H_a), 8.74 (s, 2H, H_f), 8.72 (dd, J_1 = 4.6 Hz, J_2 = 1.1 Hz, 2H, H_b), 8.48 (ddd, J_1 = 8.3 Hz, J_2 = 2.3 Hz, J_3 = 1.4 Hz, 2H, H_d), 8.13 (dd, J_1 = 6 Hz, J_2 = 3.6 Hz, 2H, H_g), 7.85 (dd, J_1 = 8.2 Hz, J_2 = 4.7 Hz, 2H, H_c), 7.66 (dd, J_1 = 6 Hz, J_2 = 3.5 Hz, 2H, H_h) *ppm*; ^{13}C NMR (125 MHz, DMSO-d_6 external TMS/$CDCl_3$): δ = 154.3, 143.8, 140.8, 137.4, 132.0, 126.5, 125.5, 125.3, 124.7 *ppm*. ESI-MS: m/z = 349, 371, 387, 697, and 719 corresponding to $(M + H)^+$, $(M + Na)^+$, $(M + K)^+$, $(2M + H)^+$ and $(2M + Na)^+$, respectively. Anal. Calcd for $C_{18}H_{16}N_6O_2(H_2O)_2$: C, 56.24; H, 5.24; N, 21.86. Found: C, 56.32; H, 5.02; N, 21.72.

1,1′-(1,3-Phenylene)bis(3-(pyridin-3-yl)urea) ***L2***. Yield: (435 mg, 74%). ^1H NMR (500 MHz, DMSO-d_6 external TMS/$CDCl_3$): δ = 9.40 (s, 2H, H_e), 9.31 (s, 2H, H_f), 9.16 (bs, 2H, H_a), 8.74 (bs, 2H, H_b), 8.48 (d, J = 8.3 Hz, 2H, H_d), 8.24 (s, 1H, H_g), 7.86 (dd, J_1 = 7.7 Hz, J_2 = 4.4 Hz, 2H, H_c), 7.73 (t, J = 8 Hz, 1H, H_i), 7.64 (dd, J_1 = 8 Hz, J_2 = 1.6 Hz, 2H, H_h) *ppm*; ^{13}C NMR (125 MHz, DMSO-d_6 external TMS/$CDCl_3$): δ = 153.0, 143.3, 140.5, 140.4, 136.9, 129.7, 125.6, 124.1, 112.6, 108.7 *ppm*.

1,1′-(1,4-Phenylene)bis(3-(pyridin-3-yl)urea) ***L3***. Yield: (425 mg, 72%). ^1H NMR (500 MHz, DMSO-d_6 external TMS/$CDCl_3$): δ = 9.33 (s, 2H, H_e), 9.22 (s, 2H, H_f), 9.14 (d, J = 2.4 Hz, 2H, H_a), 8.71 (dd, J_1 = 4.6 Hz, J_2 = 1.3 Hz, 2H, H_b), 8.47 (ddd, J_1 = 8.3 Hz, J_2 = 2.5 Hz, J_3 = 1.5 Hz 2H, H_d), 7.92 (s, 4H, H_g), 7.84 (dd, J_1 = 8.3 Hz, J_2 = 4.6 Hz, 2H, H_c) *ppm*; ^{13}C NMR (125 MHz, DMSO-d_6 external TMS/$CDCl_3$): δ = 153.2, 143.2, 140.5, 137.1, 134.6, 125.6, 124.1, 119.8 *ppm*.

Synthesis of Binuclear Cages, 1−**3.** *General Method.* A solution of $Pd(NO_3)_2$ was prepared by a salt-metathesis reaction using $PdCl_2$ (15 mg, 0.08 mmol) and $AgNO_3$ (29 mg, 0.16 mmol) in 4 mL of DMSO. The reaction mixture was stirred at 60 °C for 1 h followed by separation of the precipitated AgCl from the desired

Scheme 1. Synthesis of the Regioisomeric Ligands (L1, L2, and L3) and Pd_2L_4-type Isomeric Cages (1, 2, and 3)

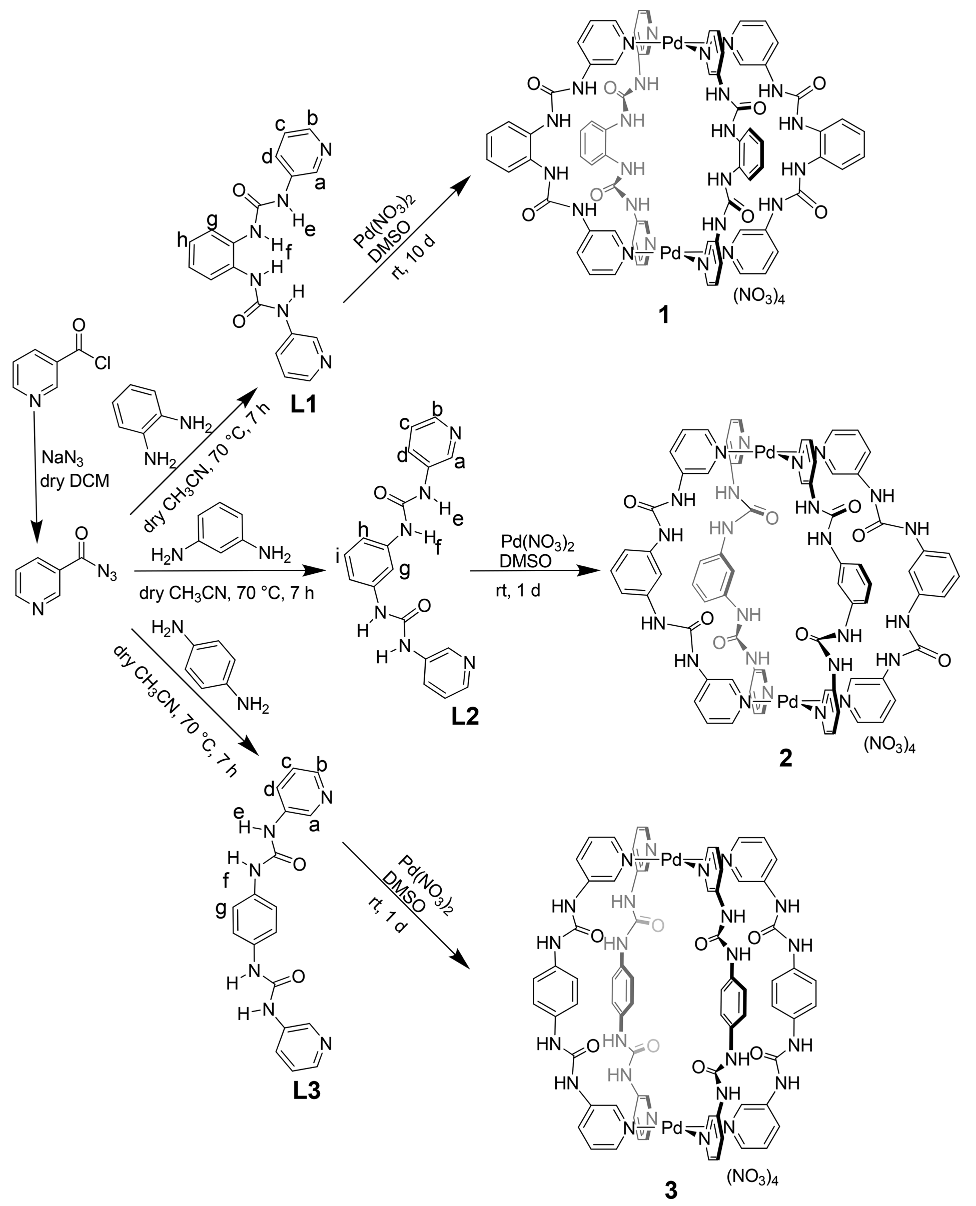

orange-red colored solution by a centrifugation method. A solution of the ligand **L1** (59 mg, 0.16 mmol) in 4.5 mL of DMSO was combined with the above-mentioned solution of $Pd(NO_3)_2$ to allow the complexation reaction. The reaction mixture was stirred at room temperature; however, during the complexation reaction a minor amount of a second crop of AgCl was also formed. The AgCl was separated from the reaction mixture by the centrifugation method to obtain a clear solution. The desired complex was precipitated from the clear solution using an excess amount of EtOAC, which was separated by filtration. The isolated solid was washed with EtOAc and dried under a vacuum to afford the cage **1** as a white solid. The cages **2** and **3** were prepared in a similar manner using **L2** and **L3**, respectively.

$[Pd_2(L1)_4](NO_3)_4$, ***1***. Yield: (52 mg, 70%). Melting point = 185 °C. ^{1}H NMR (400 MHz, DMSO-d_6 external TMS/CDCl$_3$): δ = 10.15 (s, 8H, H$_e$), 9.47 (s, 8H, H$_a$), 8.85 (d, J = 5.4 Hz, 8H, H$_b$), 8.78 (s, 8H, H$_f$), 8.63 (d, J = 8.3 Hz, 8H, H$_d$), 8.01 (dd, J_1 = 8.3 Hz, J_2 = 5.8 Hz, 8H, H$_c$), 7.94 (s, 8H, H$_g$), 7.66 (dd, J_1 = 5.6 Hz, J_2 = 3.7 Hz, 8H, H$_h$) *ppm*; ^{1}H NMR (500 MHz, DMSO-d_6 external TMS/CDCl$_3$) recorded at 70 °C: δ = 10.05 (s, 8H, H$_e$), 9.43 (d, J = 2.1 Hz, 8H, H$_a$), 8.85 (d, J = 5.4 Hz, 8H, H$_b$), 8.73 (s, 8H, H$_f$), 8.70 (d, J = 8.5 Hz, 8H, H$_d$), 8.08 (dd, J_1 = 8.5 Hz, J_2 = 5.6 Hz, 8H, H$_c$), 8.03 (dd, J_1 = 5.8 Hz, J_2 = 3.6 Hz, 8H, H$_g$), 7.68 (dd, J_1 = 6.0 Hz, J_2 = 3.5 Hz, 8H, H$_h$) *ppm*. ^{13}C NMR (125 MHz, DMSO-d_6): δ = 153.9, 145.4, 143.2, 139.6, 132.1, 131.0, 127.8, 126.3, 125.9 *ppm*; ESI-MS: *m*/*z* calculated for [**1**-2NO$_3$]$^{2+}$, 865.1604; observed, 865.1570; and calculated for [**1**-3NO$_3$]$^{3+}$, 556.1111; observed, 556.1095. Anal. Calcd for $C_{72}H_{64}N_{28}O_{20}Pd_2(DMSO)_3(H_2O)_5$: C, 43.00; H, 4.26; N, 18.00. Found: C, 42.61; H, 3.95; N, 18.43.

$[Pd_2(L2)_4](NO_3)_4$, ***2***. Yield: (50 mg, 70%). Melting point = 240 °C. ^{1}H NMR (400 MHz, DMSO-d_6 external TMS/CDCl$_3$): δ = 10.25 (bs, 8H, H$_a$), 9.71 (s, 8H, H$_e$), 9.60 (s, 8H, H$_f$), 9.51 (bs, 8H, H$_b$), 8.48 (bs, 8H, H$_d$), 8.23 (s, 4H, H$_g$), 8.15–8.11 (m, 8H, H$_c$), 7.74–7.70 (m, 12H, H$_h$ and H$_i$) *ppm*; ^{1}H NMR (500 MHz, DMSO-d_6 external TMS/CDCl$_3$) recorded at 70 °C: δ = 10.26 (s, 8H, H$_a$), 9.70 (s, 8H, H$_e$), 9.51 (s, 8H, H$_f$), 9.48 (d, J = 5.4 Hz, 8H, H$_b$), 8.49 (d, J = 7.1 Hz, 8H, H$_d$), 8.24 (d, J = 1.0 Hz, H$_g$), 8.11 (dd, J_1 = 8.4 Hz, J_2 = 5.6 Hz, 8H, H$_c$), 7.73–7.70 (m, 12H, H$_h$ and H$_i$) *ppm*. ^{13}C NMR (125 MHz, DMSO-d_6): δ = 152.5, 145.2, 141.3, 140.1, 139.2, 130.4, 130.2, 127.4, 113.6, 108.9 *ppm*; ESI-MS: *m*/*z* calculated for [**2**-2NO$_3$]$^{2+}$, 865.1604; observed, 865.1589; calculated for [**2**-3NO$_3$]$^{3+}$, 556.1111; observed, 556.1105; and calculated for [**2**-4NO$_3$]$^{4+}$, 401.5865; observed, 401.5855. Anal. Calcd for $C_{72}H_{64}N_{28}O_{20}Pd_2(DMSO)_3(H_2O)_2$: C, 44.09; H, 4.08; N, 18.46. Found: C, 44.29; H, 3.76; N, 18.34.

[Pd$_2$(L3)$_4$](NO$_3$)$_4$, ***3***. Yield: (61 mg, 83%). Melting point = 220 °C. ^{1}H NMR (500 MHz, DMSO-d_6 external TMS/CDCl$_3$): δ = 10.74 (s, 8H, H$_a$), 9.75 (s, 8H, H$_e$), 9.68 (d, J = 5.4 Hz, 8H, H$_b$), 9.52 (s, 8H, H$_f$), 8.11 (dd, J_1 = 8.2 Hz, J_2 = 5.7 Hz, 8H, H$_c$), 8.06 (s, 16H, H$_g$), 8.00 (d, J = 8.3 Hz, 8H, H$_d$) *ppm*; ^{13}C NMR (125 MHz, DMSO-d_6): δ = 152.4, 144.6, 141.5, 139.3, 134.4, 129.4, 127.1, 119.8 *ppm*; ESI-MS: m/z calculated for [**3**-2NO$_3$]$^{2+}$, 865.1604; observed, 865.1572; calculated for [**3**-3NO$_3$]$^{3+}$, 556.1111; observed, 556.1094; and calculated for [**3**-4NO$_3$]$^{4+}$, 401.5865; observed, 401.5853. Anal. Calcd for $C_{72}H_{64}N_{28}O_{20}Pd_2(DMSO)_5(H_2O)_4$: C, 42.51; H, 4.44; N, 16.93. Found: C, 42.99; H, 4.20; N, 16.40.

Crystallographic Data Collection and Refinement. X-ray data were collected with a Bruker AXS Kappa Apex II CCD diffractometer equipped with graphite monochromated Mo$_{K\alpha}$ (λ = 0.7107 Å) radiation. A crystal fixed at the tip of the glass fiber was mounted on the goniometer head and was optically centered. The automatic cell determination routine, with 36 frames at three different orientations of the detector was employed to collect reflections, and the program APEXII-SAINT (Bruker, 2008) was used for finding the unit cell parameters.[42] A 4-fold redundancy per reflection was utilized for achieving good absorption correction using a multiscan procedure. Besides absorption, Lorentz polarization and decay correction were applied during data reduction. The program SADABS (Bruker, 2008) was used for absorption correction using the multiscan procedure. The structures were solved by direct methods using SHELXS-97, (Sheldrick, 2008)[43] and refined by full-matrix least-squares techniques using the SHELXL-97 (Sheldrick, 2013)[44] computer program. All hydrogen atoms were fixed at chemically meaningful positions, and riding model refinement was applied. Molecular graphics were generated using Mercury programs. For compounds **1**−**3**, PLATON/SQUEEZE (Spek, 2009)[45] was employed to remove the excess electron density resulting from the disordered sea of solvent molecules, subsequently resulting in improved refinement.

X-ray diffraction quality single crystals of ligand **L1** were obtained by slow evaporation of a solution of **L1** in methanol−water (1:1). The compound was crystallized in the triclinic crystal system with $P\bar{1}$ space group. The asymmetric unit of the structure is composed of one unit of ligand and two molecules of water. X-ray diffraction quality single crystals of **1**·1.5(DMSO)·2(H$_2$O)·(DCE) were obtained by slow vapor diffusion of 1,2-dichloroethane into a solution of cage, **1** in DMSO. The cage molecule was crystallized in the monoclinic crystal system with $P2_1/n$ space group. The asymmetric unit contains half of the molecule of **1** (i.e., two **L1**, one palladium(II) ion, and two nitrate anions), two DMSO (one molecule with full and other with half occupancies), two H$_2$O molecules, and one dichloroethane disordered over two sites (with half occupancies each). X-ray diffraction quality single crystals of **2**·4(DMSO)·3(dioxane) were obtained by slow vapor diffusion of 1,4-dioxane into a solution of cage, **2** in DMSO. The cage molecule was crystallized in the triclinic crystal system with $P\bar{1}$ space group. The asymmetric unit contains two separate units of half of the molecule of **2**, (i.e., four **L2**, two palladium(II) ion, and four disordered nitrate anions), four DMSO, and three dioxane molecules (one dioxane with full occupancy, two dioxane with half occupancy, and two dioxane as half molecule). X-ray diffraction quality single crystals of **3**·4(DMSO)·(dioxane) were obtained by slow vapor diffusion of 1,4-dioxane into a solution of cage, **3** in DMSO. The cage molecule was crystallized in the orthorhombic crystal system with $P2_12_12$ space group. The asymmetric unit contains half of the molecule of **3** (i.e., two **L3**, one palladium(II) ion, and two nitrate anions), two DMSO (one is disordered), and one dioxane molecule (half occupancy).

Gas Adsorption. Gas adsorption measurements were performed using a BelSorpmax instrument (Bel Japan). 99.999% purity CO$_2$ and N$_2$ (employed as an inert gas) were used for sorption studies. Prior to sorption measurements, powdered samples of the cages, **1**−**3** were immersed in CH$_3$CN in separate containers for 1 day followed by centrifugation and decantation of solvent. The same procedure was repeated three times, and the resulting solid samples were dried under a vacuum to remove residual solvent molecules. The activated samples of **1**−**3** were heated at 105 °C overnight.

■ RESULTS AND DISCUSSION

Ligands (L1−L3). The ligands were prepared by condensation of freshly prepared nicotinoyl azide with appropriate diaminobenzene (Scheme 1). The peaks observed in ^{1}H and ^{13}C NMR spectra of the ligands were assigned by analyzing their COSY and HSQC spectra (see Supporting Information, Figures S4−S7, S9−S12, and S14−S17). The assignment of urea NH protons could be completed only after analyzing the NOESY data of the compounds (see Supporting Information, Figures S8, S13, and S18). Formation of the new ligand **L1** was further supported by electrospray ionization mass spectrometry (ESI-MS) (see Supporting Information, Figure S34), and its structure was also obtained using a single-crystal X-ray diffraction technique.

The nonchelating bidentate ligands **L1**, **L2**, and **L3** are 3-pyridyl appended and regioisomeric in nature. The spacer units of the ligands can be best described structurally as *ortho*, *meta*, and *para*-phenylene-diurea for **L1**−**L3**, respectively. The central phenylene and either of the terminal 3-pyridyl are flanked by urea moiety. The strong preference of *trans/trans* conformations around (C)$_{\text{urea}}$−(N)$_{\text{urea}}$ bonds in acyclic 1,3-disubstituted urea moieties is well-known, wherein the carbonyl bond and N−H bonds are oriented in opposite directions.[46] However, a large number of conformational isomers are reasoned for each of the regioisomers considering rotation around (C)$_{\text{phenylene}}$−(N)$_{\text{urea}}$ as well as (C)$_{\text{pyridyl}}$−(N)$_{\text{urea}}$ bonds.

The positions of pyridine nitrogen atoms and urea oxygen atoms present in a sequence (say, from top to bottom in the drawing), i.e., (N)pyridyl----(O)urea-----(O)urea-----(N)-pyridyl are considered as reference points to define the conformers.[41,47,48] The terms *syn* and *anti* are used to name the conformers of a given ligand as identified in three regions of its backbone, namely, (i) (N)pyridyl----(O)urea; (ii) (O)urea-----(O)urea; and (iii) (O)urea-----(N)pyridyl. The plausible conformers of the ligands are provided in Supporting Information, Figures S1, S2, and S3 that are shown using planar structures for convenience. However, global non-planarity due to torsion around the urea substructure, in the solid state, is an usual phenomenon.[49] The conformations of the bound ligands observed in the crystal structure of corresponding Pd$_2$L$_4$ complexes are approximately comparable to drawings shown in Figure 1 and Scheme 1(e.g., *anti-syn-anti* form of **L1** is observed in the structure of **1**). The possibilities of slow/fast conformational changes in the solution state for the bound ligand moieties should not be discarded.

Binuclear Pd$_2$L$_4$-type Cages (1−3). Combination of palladium(II) with the bidentate ligands **L1**, **L2**, and **L3** (at 2:4 ratios) in separate experiments afforded Pd$_2$L$_4$ type binuclear cages **1**, **2**, and **3**, respectively. The complexation reactions were performed in DMSO at room temperature (Scheme 1), and the targeted compounds were precipitated by addition of excess ethyl acetate. All the isolated cages were characterized by various spectroscopic techniques (see Supporting Information, Figures S19−S33 and S35−S37), including ^{1}H NMR, ^{13}C NMR, COSY, HSQC, NOESY, ESI-MS, and single crystal X-ray diffraction techniques. The assignment of urea NH protons could be completed only after analyzing the NOESY data of the compounds.

A stacking diagram of the ^{1}H NMR spectra of the ligands (**L1**−**L3**) and the corresponding cages (**1**−**3**) recorded in DMSO-d_6 is presented in Figure 2. While the signals of free

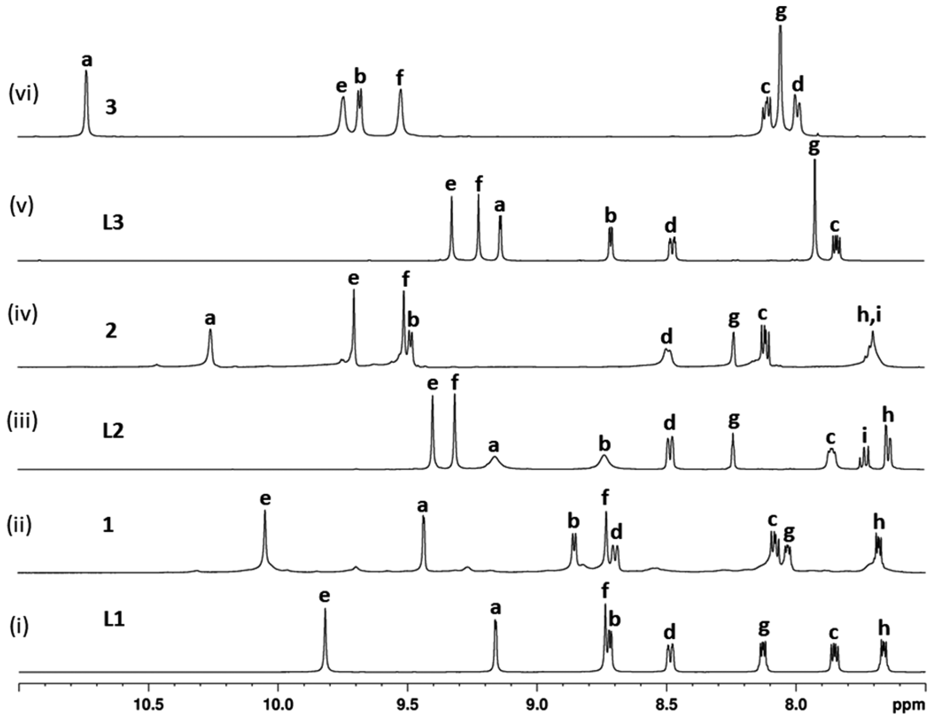

Figure 2. 500 MHz ^{1}H NMR spectra in DMSO-d_6 at room temperature (TMS as external standard) for (i) **L1**; (ii) $[Pd_2(\mathbf{L1})_4](NO_3)_4$, **1** recorded at 70 °C; (iii) **L2**; (iv) $[Pd_2(\mathbf{L2})_4](NO_3)_4$, **2** recorded at 70 °C; (v) **L3**; and (vi) $[Pd_2(\mathbf{L3})_4](NO_3)_4$, **3**. (For the designation of the protons, i.e., a, b, c, etc., see Scheme 1.)

ligand disappeared due to the complexation, a new set of signals assignable to a coordination complex was observed in each case. The signals of the complex **3** are sharp, indicating a single discrete species. However, the signals of **1** and **2** were found to be somewhat broad when the spectra were recorded at room temperature, more so for **2** (see Supporting Information, Figures S19, S19a, S24, and S24a), whereas sharp signals were observed when recorded at 70 °C (see Figure 2(ii), (iv)). Slow conformational changes at the ligand backbone could be the reason behind the signal broadening. The change in the chemical shift ($\Delta\delta$) values for the pyridyl and urea signals of the cages (H_a to H_f) as compared to the free ligands is summarized in Table S1 (see Supporting Information). The ^{1}H NMR spectra of all cages showed complexation induced downfield shift for the signals of pyridyl protons that are close to the metal binding sites (H_a and H_b). It is interesting to note that the magnitude of the downfield shift for H_a and H_b in **1** is relatively small; also the signal of H_d in **3** is found to be upfield shifted.

The Pd_2L_4 compositions of the cages (**1**−**3**) were further supported by electrospray ionization mass spectrometry (ESI-MS). The peaks at m/z = 865.1570 and 556.1095 for $[\mathbf{1}\text{-}2NO_3]^{2+}$ and $[\mathbf{1}\text{-}3NO_3]^{3+}$; m/z = 865.1589, 556.1105, and 401.5855 for $[\mathbf{2}\text{-}2NO_3]^{2+}$, $[\mathbf{2}\text{-}3NO_3]^{3+}$, and $[\mathbf{2}\text{-}4NO_3]^{4+}$; m/z = 865.1604, 556.1094, and 401.5853 for $[\mathbf{3}\text{-}2NO_3]^{2+}$, $[\mathbf{3}\text{-}3NO_3]^{3+}$, and $[\mathbf{3}\text{-}4NO_3]^{4+}$ (see Supporting Information, Figures S35−S37) confirmed the molecular compositions. The experimental isotopic pattern and the peak positions corresponding to the cationic fragments (generated due to the loss of counteranions) are in good agreement with the corresponding calculated patterns (see Supporting Information, Figures S35a-S35b; S36a-S36c; S37a-S37c).

Crystal Structure of L1·2H$_2$O. The crystal structure of ligand **L1** shows that one of the pyridyl-urea arms has a *syn*-conformation and remained almost coplanar with the central phenylene moiety where the dihedral angle of urea-phenylene planes is −2° and that of urea-pyridyl planes is −9°. However, the other arm has an *anti*-conformation and disposed almost perpendicular with respect to the phenylene plane where the dihedral angle of urea-phenylene planes is 84° and that of urea-pyridyl planes is −11°. Thus, the conformation of the ligand-substructure by considering both of the $(O)_{urea}$ atoms is somewhat gauche type, and overall a *syn-gauche-anti* conformation is observed for **L1** in the solid state (Figure 3a). Existence of this conformation in the solid state is probably influenced by the packing of the molecules.

The two water molecules are part of a "water-tetramer core", which is further stabilized by H-bond donors like $(H)_{urea}$, and acceptors like $(O)_{urea}$ and $(N)_{pyridine}$ originated from six different strands of ligands as shown in Figure 3b. Intermolecular H-bonding, $\pi-\pi$ stacking, and CH-π stacking interactions generated a chainlike arrangement in one dimension as shown in Figure 3c. A given one-dimensional chain possesses further interactions with neighboring chains. Crystallographic data and structure refinement parameters for the ligand **L1** are summarized in Table S2 (see Supporting Information).

Crystal Structures of the Cages. Single crystal of the complexes **1**, **2**, and **3** were obtained from their DMSO solutions by vapor diffusion methods. Structures of the cationic cages are shown side by side in Figure 4 for comparison. Two square planar palladium(II) centers are bridged by four ligand strands in each cage. Further description is provided in later paragraphs. Crystallographic data and structure refinement parameters for the cages (**1**−**3**) are summarized in Table S2 (see Supporting Information).

$[Pd_2(L1)_4](NO_3)_4\cdot1.5(C_2H_6SO)\cdot2(H_2O)\cdot(C_2H_4Cl_2)$. The crystal structure of cage **1** shows that one of the PdN_4 planes

DOI: 10.1021/acs.inorgchem.8b01884
Inorg. Chem. XXXX, XXX, XXX−XXX

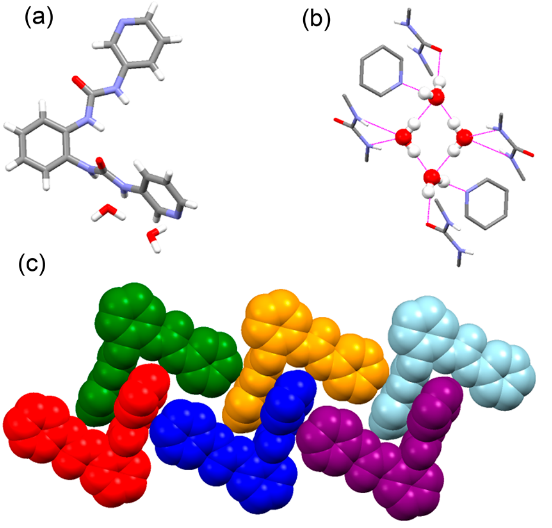

Figure 3. Crystal structure of **L1** showing (a) the asymmetric unit **L1**·$2H_2O$, (b) tetrameric water cluster found in lattice, and (c) one-dimensional view of intermolecular interactions.

is vertically above the other one, and the nonbonded distance between the two metal centers was found to be 10.5 Å. The conformation of the bound ligand moieties, more appropriately, is *anti*−*gauch*−*anti* owing to some torsion between the urea versus pyridyl and urea versus phenylene. All 16 NH groups of eight urea moieties are oriented endohedrally, thus making the cage suitable for anion encapsulation. The NH groups of eight urea moieties of $[Pd_2(\mathbf{L1})_4]^{2+}$ are involved in H-bonding interactions separately with eight chemical entities (Figure 5a). These are four counteranions (i.e., nitrate), two water molecules and two DMSO molecules (half occupancy each). Two more water molecules are buried deep in the cavity though not directly connected with urea H.

$[Pd_2(L2)_4](NO_3)_4·4(C_2H_6SO)·3(C_4H_8O_2)$. The crystal structure of cage **2** shows that one of the PdN_4 planes is above the other one but parallel displaced by approximately 10°, and the nonbonded distance between the metal centers was found to be 13.1 Å (longer than that of **1**). The conformation of the bound ligand moieties is close to *syn*−*anti*−*anti*. For any of the ligand strands, the NH groups of one of the urea moieties are endohedrally located, whereas that of the other are exohedrally located. In the cage architecture, each of the four ligand strands has two neighboring ligand strands disposed in a *cis* manner and one ligand strand is disposed in a *trans* manner. Let us consider two ligand strands that are located *trans* to each other and compare the two urea moieties located in diagonally opposite positions (belonging to different ligand strands). It can be seen that NH protons of the diagonally located urea moieties are either all endohedral or all exohedral. The above description defined the positions of all eight urea units of the cage. The endohedral NH groups belonging to four urea moieties of $[Pd_2(\mathbf{L2})_4]^{2+}$ are involved in H-bonding interactions with only two counteranions (i.e., nitrate) where a pair of urea moieties are bridged by a nitrate ion (Figure 5b). The endohedral NH groups are however pointed toward the window of the cage, and the corresponding bound nitrates are located at the window. Thus, the central cavity is available for solvent inclusion. However, the exohedral NH groups belonging to four urea moieties bind with two nitrate ions and two DMSO molecules. The inner cavity of the cage is found to accommodate two more DMSO molecules probably by electrostatic interaction of $(O)_{DMSO}$ with metal ions and several CH---O interactions using $(O)_{urea}$ and $(H)_{DMSO}$ to fill the space.

$[Pd_2(L3)_4](NO_3)_4·4(C_2H_6SO)·(C_4H_8O_2)$. The crystal structure of cage **3** shows that one of the PdN_4 planes is vertically above the other one, and the nonbonded distance between the metal centers was found to be 14.2 Å (longer than that of **1** and **2**). The conformation of the bound ligand moieties is close to *syn*−*syn*−*syn*. All the 16 NH groups of eight urea moieties are oriented exohedrally, thus making the outside edge of the cage suitable for interaction with anions. The interaction of the cage with compatible chemical entities is shown in Figure 5c. The inner cavity of the cage is found to accommodate two DMSO molecules probably by electrostatic interaction of $(O)_{DMSO}$ with metal ions and several CH---O interactions using $(O)_{urea}$ and $(H)_{DMSO}$ to fill the space. In fact, the NH groups of eight urea moieties of $[Pd_2(\mathbf{L3})_4]^{2+}$ are involved in H-bonding interactions separately with eight nitrate ions. There are only four anions in the molecular formula of a cage molecule. The presence of eight anions around a cage can be explained very easily by analyzing the packing diagram as discussed in the next section.

Intermolecular Interactions of the Cages in the Solid State. Packing diagrams from the crystal structures of the cages were generated and provided in the Supporting Information (see Figures S47, S48, and S49) that showed the existence of anions/solvents filled pores. It should be possible to activate the compounds (removal of solvents) and use the pores for gas adsorption study. However, the nature of intermolecular interactions and the nature of intramolecular/intermolecular pores could possibly change upon activation. The packing diagram of cage **3** possesses unique structural features and is discussed below.

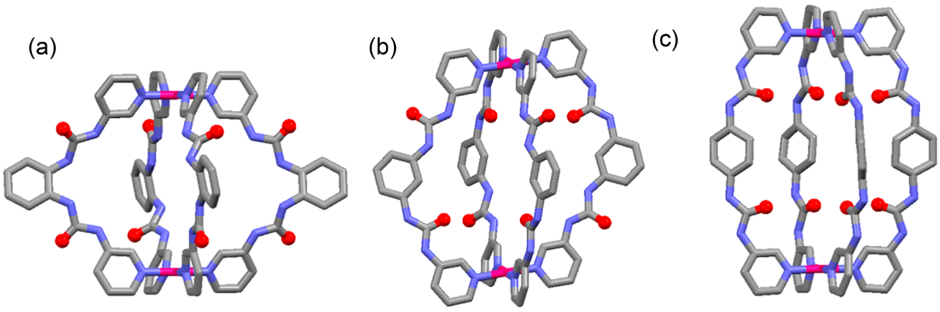

Figure 4. Crystal structure of the cages (a) **1**·1.5(DMSO)·2(H_2O)·(DCE), (b) **2**·4(DMSO)·3(dioxane), and (c) **3**·2(DMSO)·(dioxane). The counteranions, hydrogen, and solvent molecules are not shown for clarity.

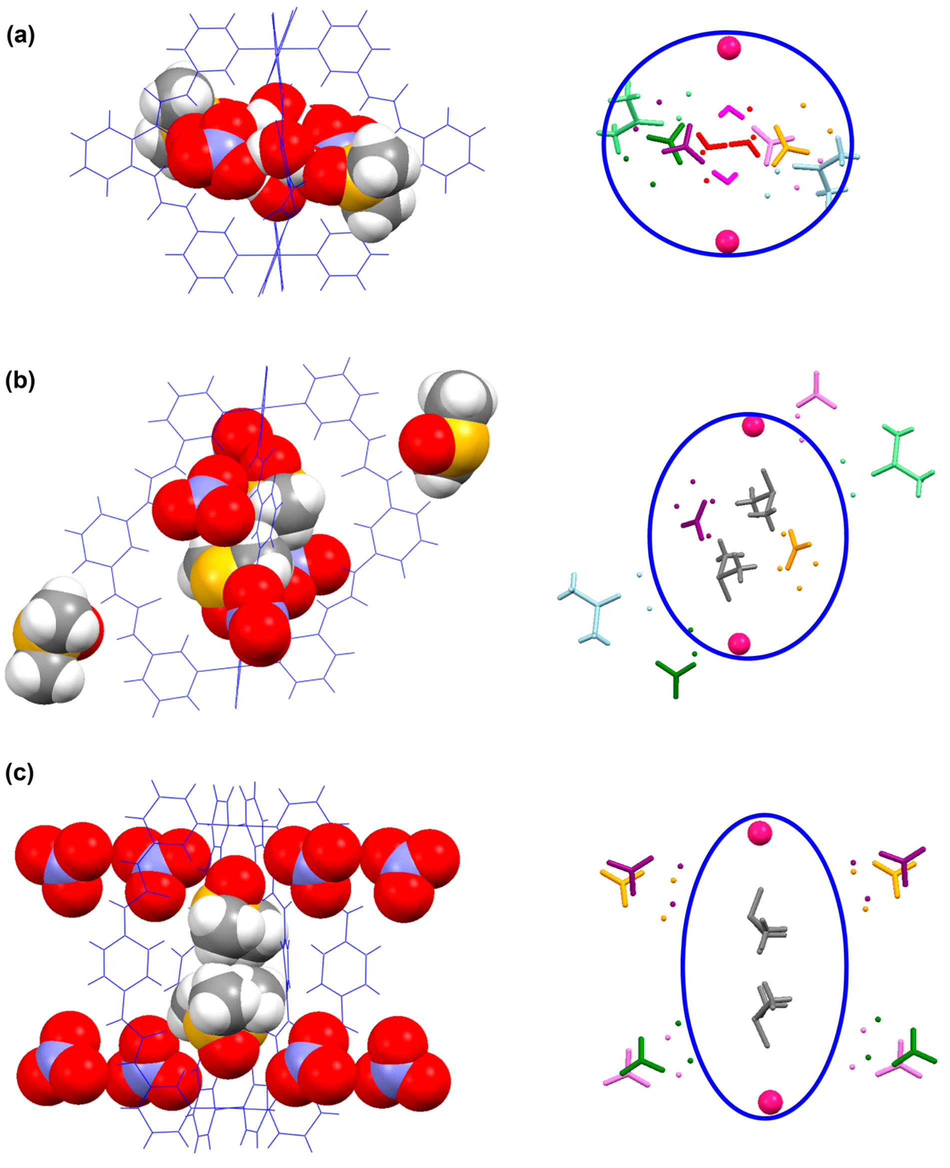

Figure 5. Crystal structures showing (a) endohedral binding of 4(NO_3), 4(H_2O), 2(DMSO) by $[Pd_2(\mathbf{L1})_4]^{2+}$ (b) endohedral binding of 2(NO_3), 2(DMSO); exohedral binding of 2(NO_3), 2(DMSO), by$[Pd_2(\mathbf{L2})_4]^{2+}$, and (c) endohedral binding of 2(DMSO); exohedral binding of 4(NO_3) by $[Pd_2(\mathbf{L3})_4]^{2+}$. Blue enclosure and colored dots shown in the right-hand side figures represent cage and $(H)_{urea}$, respectively.

Anion Supported Intermolecular Interactions in 3. As explained above, the counteranions of the cationic cage of $[Pd_2(\mathbf{L3})_4]^{2+}$ are located at fixed sites at the periphery of the cage, and the inner cavity is free of anions, though solvent molecules are trapped. Investigation of the packing diagram in the crystal structure of **3** revealed interesting anion bridged arrangements as shown in Figure 6. A pair of ligand strands of a cage unit that are located *cis* to each other and another such *cis*-pair of a neighboring cage are bridged by four nitrate moieties to create a tubular cavity. The other pairs of ligand strands are further connected in a similar manner linearly to afford a poly-cage chain. Thus, in addition to the anion free inherent cavity of cage **3** one could see anion free tubular cavities created due to the nitrate bridged arrangements. While the nonbonded distance between the metal centers of a cage unit is 14.2 Å, such a distance between the metal centers of two neighboring cages is also similar (14.3 Å). A given poly-cage chain possesses further interactions with four neighboring chains through weak interactions.

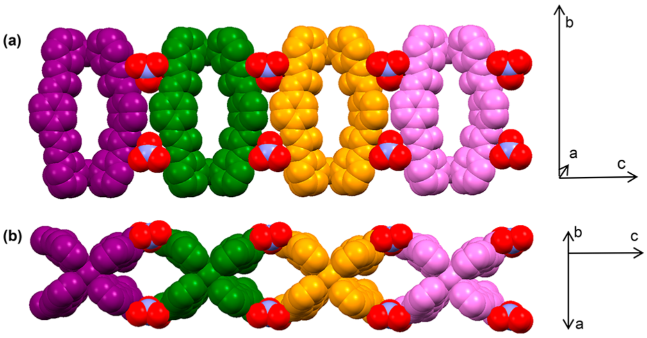

Figure 6. Two views of the packing diagram to illustrate the nitrate bridging of one unit of $[Pd_2(\mathbf{L3})_4]^{2+}$ with two such units. Hydrogen atoms and solvent molecules are omitted for clarity.

Gas Adsorption Studies. It may be noted that metal−organic frameworks (MOFs)[50−58] and covalent organic frameworks (COFs)[59−65] have been extensively investigated for gas adsorption studies, whereas self-assembled discrete coordination cages for gas adsorption is employed only recently.[8] Prior to the adsorption study, the thermal stability of the activated powdered samples of cages **1**−**3** was probed by the TGA technique, which showed comparable thermal stabilities for all the cages. The TGA curves of **1**, **2**, and **3** below 100 °C showed weight losses of 2.7% (calcd. 2.6%), 6.5% (calcd. 6.4%), and 7.4% (calcd. 7.3%), respectively, that are consistent with losses of 1 CH_3CN and 0.5 H_2O for cage **1**; 2 CH_3CN and 2.5 H_2O for cage **2**; and 2 CH_3CN and 3.5 H_2O for cage **3**. All the cage materials were found to be stable up to 200 °C, and further heating resulted in gradual decomposition (see Supporting Information, Figures S42, S43, and S44).

Preliminary gas adsorption studies were carried out using activated samples of **1**, **2**, and **3**. The powdered samples were immersed in CH_3CN for 3 days to exchange the solvents with a higher boiling point (particularly DMSO) with the solvent of lower boiling point, i.e., CH_3CN. The sample was then separated by filtration and dried under a vacuum for 1 day to remove residual solvents.

The CH_3CN exchanged sample of the cage materials, **1**−**3** was activated at 105 °C for overnight under a vacuum for the gas adsorption study. The CO_2 adsorption isotherms were recorded for all the three cages, **1**−**3** at 273 K (see Supporting Information, Figure S45) and 298 K (Figure 7). The uptake amount for cage **2** was found to be substantially higher than the other two cages (**1** and **3**) at both 273 and 298 K. This difference in uptake amounts is probably related to the orientation of the linkers in the cavity, both in terms of accessibility to the functional sites and the extent of pore windows. The complexation of pyridine groups with metal ion and electron withdrawing nature of the urea moieties are the possible forces that would make the $(\text{pyridine})_\alpha$ and phenylene protons electron deficient. The urea protons when available are also potential binding sites. These electron deficient protons will possibly bind with CO_2. Further investigations are required to understand the mechanism of gas adsorption by these cages. Nevertheless, preliminary data on the adsorption behavior demonstrate the effect of ligand isomerization toward influencing the adsorption properties in such coordination cages.

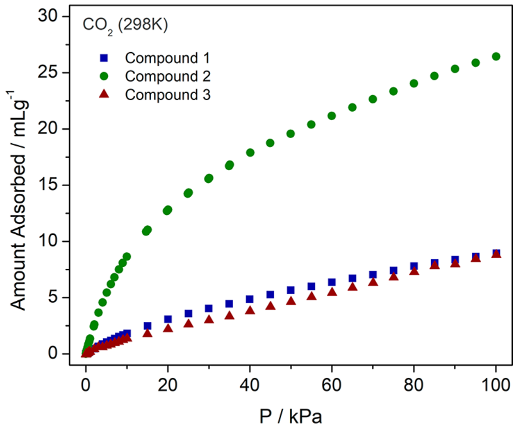

Figure 7. CO_2 adsorption isotherms recorded at 298 K for compound **1** (blue), compound **2** (green), and compound **3** (red).

Our best performing cage, i.e., $[Pd_2(\mathbf{L2})_4](NO_3)_4$, **2**, was found to adsorb ∼2.1 mol of CO_2 per mol of cage at 298 K and 100 kPa. Under similar conditions, a previously reported Pd_2L_4 type cage adsorbed 1.4 mol of CO_2 per mol of cage.[8] The computed heat of adsorption at zero loading values for the cages **1**, **2**, and **3** are 44.05, 45.74, and 31.38 kJ/mol, respectively (see Supporting Information, Figure S46). The high values indicated supportive roles of the functional sites toward the adsorption of polar CO_2. It is noteworthy to mention that the heat of adsorption is much higher than those reported previously (range: 25−35 kJ/mol).[8] The comparison re-emphasizes the superior roles of the functional groups in our Pd(II)-cages.

■ CONCLUSIONS

Complexation of palladium(II) nitrate with a set of regioisomeric nonchelating bidentate ligands (**L1**, **L2**, and **L3**) afforded isomeric cages (**1**, **2**, and **3**) of Pd_2L_4 formulation. The ligands employed are 3-pyridyl appended that are crafted with 1,2 or 1,3 or 1,4phenylene-diurea functionalities as spacers for **L1**, **L2**, and **L3**, respectively. Although the conformation of the ligands in their coordinated forms are found to be different in different cages, the cages are isomeric. Thus, ligand-isomerism in coordination cages was illustrated. The number of nitrates accommodated in the cavity of the cages is controlled by the conformation of the bound ligand (four for **1**, two for **2**, and none for **3**). Essentially the enohedral/exohedral dispositions of the $(H)_{\text{urea}}$ atoms are responsible for the location of the bound nitrates. The isomeric cages in the solid state displayed adsorption of CO_2, and the nature of adsorption is influenced by the isomers where cage **2** displayed superior binding abilities compared to the other cages.

■ ASSOCIATED CONTENT

Supporting Information

The Supporting Information is available free of charge on the ACS Publications website at DOI: 10.1021/acs.inorg-chem.8b01884.

1D and 2D NMR and ESI-MS spectra, TGA curves, CO_2 adsorption isotherm plots (PDF)

Accession Codes

CCDC 1854022−1854025 contain the supplementary crystallographic data for this paper. These data can be obtained free of charge via www.ccdc.cam.ac.uk/data_request/cif, or by emailing data_request@ccdc.cam.ac.uk, or by contacting The Cambridge Crystallographic Data Centre, 12 Union Road, Cambridge CB2 1EZ, UK; fax: +44 1223 336033.

■ AUTHOR INFORMATION

Corresponding Author

*E-mail: dillip@iitm.ac.in.

ORCID

Dillip Kumar Chand: 0000-0003-1115-0138

Notes

The authors declare no competing financial interest.

■ ACKNOWLEDGMENTS

The authors thank the SERB, Government of India (Project No. EMR/2017/002262), for financial support. D.H. thanks CSIR, New Delhi, India, for a fellowship. We gratefully acknowledge the NMR, ESI-MS (DST-FIST funded), TGA, and single crystal X-ray diffractometer facility at the Department of Chemistry, IIT Madras. We sincerely thank Dr. Sujit

K. Ghosh and Mr. Aamod V. Desai (IISER, Pune) for providing gas adsorption data and helpful discussion.

DEDICATION

This article is dedicated to Prof. Vadapalli Chandrasekhar on the occasion of his 60th birthday.

REFERENCES

(1) Clever, G. H.; Punt, P. Cation-Anion Arrangement Patterns in Self-Assembled Pd_2L_4 and Pd_4L_8 Coordination Cages. *Acc. Chem. Res.* **2017**, *50*, 2233−2243.

(2) Vasdev, R. A. S.; Preston, D.; Crowley, J. D. Multicavity Metallosupramolecular Architectures. *Chem. - Asian J.* **2017**, *12*, 2513−2523.

(3) Schmidt, A.; Casini, A.; Kühn, F. E. Self-assembled M_2L_4 coordination cages: Synthesis and potential applications. *Coord. Chem. Rev.* **2014**, *275*, 19−36.

(4) Han, M.; Engelhard, D. M.; Clever, G. H. Self-assembled coordination cages based on banana-shaped ligands. *Chem. Soc. Rev.* **2014**, *43*, 1848−1860.

(5) Harris, K.; Fujita, D.; Fujita, M. Giant hollow M_nL_{2n} spherical complexes: structure, functionalisation and applications. *Chem. Commun.* **2013**, *49*, 6703−6712.

(6) Debata, N. B.; Tripathy, D.; Chand, D. K. Self-assembled coordination complexes from various palladium(II) components and bidentate or polydentate ligands. *Coord. Chem. Rev.* **2012**, *256*, 1831−1945.

(7) Ganta, S.; Chand, D. K. Multi-Stimuli-Responsive Metallogel Molded from a Pd_2L_4-Type Coordination Cage: Selective Removal of Anionic Dyes. *Inorg. Chem.* **2018**, *57*, 3634−3645.

(8) Preston, D.; White, K. F.; Lewis, J. E. M.; Vasdev, R. A. S.; Abrahams, B. F.; Crowley, J. D. Solid-State Gas Adsorption Studies with Discrete Palladium(II) $[Pd_2(L)_4]^{4+}$ Cages. *Chem. - Eur. J.* **2017**, *23*, 10559−10567.

(9) Li, Y.-H.; Zhang, Y.; Legrand, Y.-M.; van der Lee, A.; Jiang, J.-J.; Chen, C.-X.; Su, C.-Y.; Barboiu, M. Hydrophobic metallo-supramolecular Pd_2L_4 cages for zwitterionic guest encapsulation in organic solvents. *Dalton Trans.* **2017**, *46*, 15204−15207.

(10) Löffler, S.; Lübben, J.; Wuttke, A.; Mata, R. A.; John, M.; Dittrich, B.; Clever, G. H. Internal dynamics and guest binding of a sterically overcrowded host. *Chem. Sci.* **2016**, *7*, 4676−4684.

(11) Bandi, S.; Chand, D. K. Cage-to-Cage Cascade Transformations. *Chem. - Eur. J.* **2016**, *22*, 10330−10335.

(12) Yamashina, M.; Sei, Y.; Akita, M.; Yoshizawa, M. Safe storage of radical initiators within a polyaromatic nanocapsule. *Nat. Commun.* **2014**, *5*, 4662−4668.

(13) Desmarets, C.; Gontard, G.; Cooksy, A. L.; Rager, M. N.; Amouri, H. Encapsulation of a Metal Complex within a Self-Assembled Nanocage: Synergy Effects, Molecular Structures, and Density Functional Theory Calculations. *Inorg. Chem.* **2014**, *53*, 4287−4294.

(14) Kishi, N.; Li, Z.; Sei, Y.; Akita, M.; Yoza, K.; Siegel, J. S.; Yoshizawa, M. Wide-Ranging Host Capability of a Pd^{II}-Linked M_2L_4 Molecular Capsule with an Anthracene Shell. *Chem. - Eur. J.* **2013**, *19*, 6313−6320.

(15) Preston, D.; McNeill, S. M.; Lewis, J. E. M.; Giles, G. I.; Crowley, J. D. Enhanced kinetic stability of $[Pd_2L_4]^{4+}$ cages through ligand substitution. *Dalton Trans.* **2016**, *45*, 8050−8060.

(16) Yu, H.-J.; Liu, Z.-M.; Pan, M.; Wu, K.; Wei, Z.-W.; Xu, Y.-W.; Fan, Y.-N.; Wang, H.-P.; Su, C.-Y. Elucidating Anion-Dependent Formation and Conversion of Pd_2L_4 and Pd_3L_6 Metal-Organic Cages by Complementary Techniques. *Eur. J. Inorg. Chem.* **2018**, *2018*, 80−85.

(17) Chand, D. K.; Biradha, K.; Fujita, M. Self-assembly of a novel macrotricyclic Pd(II) metallocage encapsulating a nitrate ion. *Chem. Commun.* **2001**, 1652−1653.

(18) McMorran, D. A.; Steel, P. J. The First Coordinatively Saturated, Quadruply Stranded Helicate and Its Encapsulation of a Hexafluorophosphate Anion. *Angew. Chem., Int. Ed.* **1998**, *37*, 3295−3297.

(19) Zhang, T.; Zhou, L.-P.; Guo, X.-Q.; Cai, L.-X.; Sun, Q.-F. Adaptive self-assembly and induced-fit transformations of anion-binding metal-organic macrocycles. *Nat. Commun.* **2017**, *8*, 15898.

(20) Han, M.; Luo, Y.; Damaschke, B.; Gómez, L.; Ribas, X.; Jose, A.; Peretzki, P.; Seibt, M.; Clever, G. H. Light-Controlled Interconversion between a Self-Assembled Triangle and a Rhombicuboctahedral Sphere. *Angew. Chem., Int. Ed.* **2016**, *55*, 445−449.

(21) Ganta, S.; Chand, D. K. Nanoscale metallogel *via* self-assembly of self-assembled trinuclear coordination rings: multi-stimuli-responsive soft materials. *Dalton Trans.* **2015**, *44*, 15181−15188.

(22) Samanta, D.; Mukherjee, P. S. Component Selection in the Self-Assembly of Palladium(II) Nanocages and Cage-to-Cage Transformations. *Chem. - Eur. J.* **2014**, *20*, 12483−12492.

(23) Suzuki, K.; Kawano, M.; Fujita, M. Solvato-Controlled Assembly of Pd_3L_6 and Pd_4L_8 Coordination "Boxes. *Angew. Chem., Int. Ed.* **2007**, *46*, 2819−2822.

(24) Chand, D. K.; Biradha, K.; Kawano, M.; Sakamoto, S.; Yamaguchi, K.; Fujita, M. Dynamic Self-Assembly of an M_3L_6 Molecular Triangle and an M_4L_8 Tetrahedron from Naked Pd^{II} Ions and Bis(3-pyridyl)-Substituted Arenes. *Chem. - Asian J.* **2006**, *1*, 82−90.

(25) Howlader, P.; Mukherjee, S.; Saha, R.; Mukherjee, P. S. Conformation-selective coordination-driven self-assembly of a ditopic donor with Pd^{II} acceptors. *Dalton Trans.* **2015**, *44*, 20493−20501.

(26) Han, M.; Michel, R.; Clever, G. H. Rational Design of a Face-Centred Square-Cuboid Coordination Cage. *Chem. - Eur. J.* **2014**, *20*, 10640−10644.

(27) Suzuki, K.; Tominaga, M.; Kawano, M.; Fujita, M. Self-assembly of an M_6L_{12} coordination cube. *Chem. Commun.* **2009**, 1638−1640.

(28) Fujita, D.; Yokoyama, H.; Ueda, Y.; Sato, S.; Fujita, M. Geometrically Restricted Intermediates in the Self-Assembly of an $M_{12}L_{24}$ Cuboctahedral Complex. *Angew. Chem., Int. Ed.* **2015**, *54*, 155−158.

(29) Sun, Q.-F.; Iwasa, J.; Ogawa, D.; Ishido, Y.; Sato, S.; Ozeki, T.; Sei, Y.; Yamaguchi, K.; Fujita, M. Self-Assembled $M_{24}L_{48}$ Polyhedra and Their Sharp Structural Switch upon Subtle Ligand Variation. *Science* **2010**, *328*, 1144−1147.

(30) Tominaga, M.; Suzuki, K.; Murase, T.; Fujita, M. 24-Fold Endohedral Functionalization of a Self-Assembled $M_{12}L_{24}$ Coordination Nanoball. *J. Am. Chem. Soc.* **2005**, *127*, 11950−11951.

(31) Tominaga, M.; Suzuki, K.; Kawano, M.; Kusukawa, T.; Ozeki, T.; Sakamoto, S.; Yamaguchi, K.; Fujita, M. Finite, Spherical Coordination Networks that Self-Organize from 36 Small Components. *Angew. Chem., Int. Ed.* **2004**, *43*, 5621−5625.

(32) Fujita, D.; Ueda, Y.; Sato, S.; Mizuno, N.; Kumasaka, T.; Fujita, M. Self-assembly of tetravalent Goldberg polyhedra from 144 small components. *Nature* **2016**, *540*, 563−566.

(33) Fujita, D.; Ueda, Y.; Sato, S.; Yokoyama, H.; Mizuno, N.; Kumasaka, T.; Fujita, M. Self-assembly of $M_{30}L_{60}$ Icosidodecahedron. *Chem.* **2016**, *1*, 91−101.

(34) Howlader, P.; Das, P.; Zangrando, E.; Mukherjee, P. S. Urea-Functionalized Self-Assembled Molecular Prism for Heterogeneous Catalysis in Water. *J. Am. Chem. Soc.* **2016**, *138*, 1668−1676.

(35) Dasary, H.; Jagan, R.; Chand, D. K. Octadecanuclear Gear Wheels by Self-Assembly of Self-Assembled "Double Saddle"-Type Coordination Entities: Molecular "Rangoli. *Chem. - Eur. J.* **2015**, *21*, 1499−1507.

(36) Marshall, L. J.; de Mendoza, J. Self-Assembled Squares and Triangles by Simultaneous Hydrogen Bonding and Metal Coordination. *Org. Lett.* **2013**, *15*, 1548−1551.

(37) Troff, R. W.; Hovorka, R.; Weilandt, T.; Lützen, A.; Cetina, M.; Nieger, M.; Lentz, D.; Rissanen, K.; Schalley, C. A. Equipping metallo-supramolecular macrocycles with functional groups: assemblies of pyridine-substituted urea ligands. *Dalton Trans.* **2012**, *41*, 8410−8420.

DOI: 10.1021/acs.inorgchem.8b01884

(38) Naranthatta, M. C.; Das, D.; Tripathy, D.; Sahoo, H. S.; Ramkumar, V.; Chand, D. K. Consequence of Presence and Absence of π-Clouds at Strategic Locations of Designed Binuclear Pd(II) Complexes on Packing: Self-Assembly of Self-Assembly by Intermolecular Locking and Packing. *Cryst. Growth Des.* **2012**, *12*, 6012−6022.

(39) Gispert, J. R. *Coordination Chemistry*; Wiley-VCH, 2008; p 98.

(40) Adarsh, N. N.; Dastidar, P. *catena*-Poly[[[triaquasulfatozinc-(II)]-μ-3,3′-bis(3-pyridyl)-1,1′-(*m*-phenylene)diurea] methanol solvate monohydrate]. *Acta Crystallogr., Sect. E: Struct. Rep. Online* **2010**, *66*, m413−m414.

(41) Byrne, P.; Turner, D. R.; Lloyd, G. O.; Clarke, N.; Steed, J. W. Gradual Transition from NH···Pyridyl Hydrogen Bonding to the NH···O Tape Synthon in Pyridyl Ureas. *Cryst. Growth Des.* **2008**, *8*, 3335−3344.

(42) *SAINT*, version 7.06a; Bruker AXS Inc.: Madison, WI, 2008.

(43) Sheldrick, G. M. A short history of SHELX. *Acta Crystallogr., Sect. A: Found. Crystallogr.* **2008**, *64*, 112−122.

(44) Sheldrick, G. M. Recent developments in SHELX. *Acta Crystallogr., Sect. A: Found. Crystallogr.* **2013**, *69*, S74.

(45) Spek, A. L. Structure validation in chemical crystallography. *Acta Crystallogr., Sect. D: Biol. Crystallogr.* **2009**, *65*, 148−155.

(46) Semetey, V.; Hemmerlin, C.; Didierjean, C.; Schaffner, A.-P.; Giner, A. G.; Aubry, A.; Briand, J.-P.; Marraud, M.; Guichard, G. Unexpected Stability of the Urea *cis-trans* Isomer in Urea-Containing Model Pseudopeptides. *Org. Lett.* **2001**, *3*, 3843−3846.

(47) Paul, M.; Dastidar, P.; Adarsh, N. N. Cu^{II} Coordination Polymers Capable of Gelation and Selective SO_4^{-2} Separation. *Cryst. Growth Des.* **2012**, *12*, 4135−4143.

(48) Adarsh, N. N.; Dastidar, P. A Borromean Weave Coordination Polymer Sustained by Urea-Sulfate Hydrogen Bonding and Its Selective Anion Separation Properties. *Cryst. Growth Des.* **2010**, *10*, 483−487.

(49) Loeffler, J. R.; Ehmki, E. S. R.; Fuchs, J. E.; Liedl, K. R. Kinetic barriers in the isomerization of substituted ureas: implications for computer-aided drug design. *J. Comput.-Aided Mol. Des.* **2016**, *30*, 391−400.

(50) Schneemann, A.; Bon, V.; Schwedler, I.; Senkovska, I.; Kaskel, S.; Fischer, R. A. Flexible metal-organic frameworks. *Chem. Soc. Rev.* **2014**, *43*, 6062−6096.

(51) Sumida, K.; Rogow, D. L.; Mason, J. A.; McDonald, T. M.; Bloch, E. D.; Herm, Z. R.; Bae, T.-H.; Long, J. R. Carbon Dioxide Capture in Metal-Organic Frameworks. *Chem. Rev.* **2012**, *112*, 724−781.

(52) Liu, J.; Thallapally, P. K.; McGrail, B. P.; Brown, D. R.; Liu, J. Progress in adsorption-based CO_2 capture by metal-organic frameworks. *Chem. Soc. Rev.* **2012**, *41*, 2308−2322.

(53) Férey, G.; Serre, C.; Devic, T.; Maurin, G.; Jobic, H.; Llewellyn, P. L.; de Weireld, G.; Vimont, A.; Daturi, M.; Chang, J.-S. Why hybrid porous solids capture greenhouse gases? *Chem. Soc. Rev.* **2011**, *40*, 550−562.

(54) Nandi, S.; Maity, R.; Chakraborty, D.; Ballav, H.; Vaidhyanathan, R. Preferential Adsorption of CO_2 in an Ultramicroporous MOF with Cavities Lined by Basic Groups and Open-Metal Sites. *Inorg. Chem.* **2018**, *57*, 5267−5272.

(55) Gupta, M.; De, D.; Tomar, K.; Bharadwaj, P. K. From Zn(II)-Carboxylate to Double-Walled Zn(II)-Carboxylato Phosphate MOF: Change in the Framework Topology, Capture and Conversion of CO_2, and Catalysis of Strecker Reaction. *Inorg. Chem.* **2017**, *56*, 14605−14611.

(56) Kanoo, P.; Haldar, R.; Reddy, S. K.; Hazra, A.; Bonakala, S.; Matsuda, R.; Kitagawa, S.; Balasubramanian, S.; Maji, T. K. Crystal Dynamics in Multi-stimuli-Responsive Entangled Metal-Organic Frameworks. *Chem. - Eur. J.* **2016**, *22*, 15864−15873.

(57) Mukherjee, S.; Desai, A. V.; More, Y. D.; Inamdar, A. I.; Ghosh, S. K. A Bifunctional Metal-Organic Framework: Striking CO_2 Selective Sorption Features along with Guest-Induced Tuning of Luminescence. *ChemPlusChem* **2016**, *81*, 702−707.

(58) Pachfule, P.; Chen, Y.; Jiang, J.; Banerjee, R. Fluorinated Metal-Organic Frameworks: Advantageous for Higher H_2 and CO_2 Adsorption or Not? *Chem. - Eur. J.* **2012**, *18*, 688−694.

(59) Zeng, Y.; Zou, R.; Zhao, Y. Covalent Organic Frameworks for CO_2 Capture. *Adv. Mater.* **2016**, *28*, 2855−2873.

(60) Hong, S.; Rohman, M. R.; Jia, J.; Kim, Y.; Moon, D.; Kim, Y.; Ko, Y. H.; Lee, E.; Kim, K. Porphyrin Boxes: Rationally Designed Porous Organic Cages. *Angew. Chem.* **2015**, *127*, 13439−13442.

(61) Zhang, G.; Mastalerz, M. Organic cage compounds-from shape-persistency to function. *Chem. Soc. Rev.* **2014**, *43*, 1934−1947.

(62) Ding, S.-Y.; Wang, W. Covalent organic frameworks (COFs): from design to applications. *Chem. Soc. Rev.* **2013**, *42*, 548−568.

(63) Feng, X.; Ding, X.; Jiang, D. Covalent organic frameworks. *Chem. Soc. Rev.* **2012**, *41*, 6010−6022.

(64) Mastalerz, M. Permanent Porous Materials from Discrete Organic Molecules-Towards Ultra-High Surface Areas. *Chem. - Eur. J.* **2012**, *18*, 10082−10091.

(65) Furukawa, H.; Yaghi, O. M. Storage of Hydrogen, Methane, and Carbon Dioxide in Highly Porous Covalent Organic Frameworks for Clean Energy Applications. *J. Am. Chem. Soc.* **2009**, *131*, 8875−8883.